INSTITUTE OF PHYSICS PUBLISHING JOURNAL OF PHYSICS: CONDENSED MATTER

J. Phys.: Condens. Matter **19** (2007) 065103 (9pp) doi:10.1088/0953-8984/19/6/065103

Reaction–diffusion fronts with inhomogeneous initial conditions

I Bena[1], **M Droz**[1], **K Martens**[1] **and Z Rácz**[2]

[1] Département de Physique Théorique, Université de Genève, CH-1211 Genève 4, Switzerland
[2] Institute for Theoretical Physics, Eötvös University, 1117 Budapest, Hungary

Received 13 July 2006
Published 22 January 2007
Online at stacks.iop.org/JPhysCM/19/065103

Abstract

Properties of reaction zones resulting from $A + B \to C$ type reaction–diffusion processes are investigated by analytical and numerical methods. The reagents A and B are separated initially and, in addition, there is an initial macroscopic inhomogeneity in the distribution of the B species. For simple two-dimensional geometries, exact analytical results are presented for the time evolution of the geometric shape of the front. We also show using cellular automata simulations that the fluctuations can be neglected both in the shape and in the width of the front.

1. Introduction

Front propagation has attracted considerable research activity during the past years. A large number of phenomena in different fields (e.g. crystal growth, chemical pattern formation, and biological invasion problems) are determined by the properties of various types of front.

An important class of problems is related to the case of front propagation into unstable states [1]. They describe situations in which the dynamics of a system is governed by a front which invades a domain in which the system is in an unstable state, leading to the onset of a new stable state (often with spatio-temporal structures present). Examples include population dynamics modelled by the extended Fisher–Kolmogorov equation [2], onset of vortices in Taylor–Couette flows [3] and of convection rolls in Rayleigh–Bénard experiments (modelled by the Swift–Hohenberg equation [4]), and phase turbulence in autocatalytic chemical reactions modelled by the Kuramoto–Sivashinsky equation [5].

Most of the studies have been addressing the properties of reaction–diffusion fronts in homogeneous media [6]. At present, however, an increasing importance is attached to the more complicated cases of fronts propagating in *inhomogeneous media*. Inhomogeneities may have different natures: chemical (related to spatial inhomogeneities in the concentration of the reagents), physical (reagents' diffusion coefficients may vary in space), geometrical (changes in the geometry of the medium), etc. Also, inhomogeneities may be either related to an intrinsic disorder present in the system, or may be created artificially. There have been both theoretical

and experimental effort in studying various situations; see e.g. [7–11]. Examples are numerous in the context of biology [12], population dynamics [13], heterogeneous catalysis [14], or heterogeneous excitable media like the photosensitive Belousov–Zhabotinsky reaction [15–17]. In particular, it was argued that under some circumstances reaction–diffusion fronts may behave like light waves when undergoing refraction and reflection [9–11].

In this paper we shall be concerned with a different class of phenomena which emerges when the unstable state is produced by reaction processes in a front moving diffusively. In the wake of the front, the dynamics of the unstable state may generate various spatio-temporal patterns. A prototype of this pattern-forming process is the Liesegang phenomenon [18][3] where a chemical reactant (called inner electrolyte) is dissolved in a gel matrix and a second reactant (outer electrolyte) diffuses in and reacts with the inner electrolyte. Under certain conditions, the dynamics of the reaction product generates a family of high-density precipitate zones whose properties obey generic laws [20] which have been understood in terms of a simple phase separation scenario [21].

Most of the Liesegang pattern studies have been made in homogeneous conditions [18], when the initial concentration of the inner electrolyte is uniform. In recent work by Grzybowski *et al* [22], however, the experiments were performed in inhomogeneous conditions (with a step-like profile in the height of the gel containing the inner electrolyte). It was argued that Liesegang bands emerging in the two regions of different thicknesses join each other at the step according to a Snell law, where the indices of refraction are related to the so-called spacing coefficients of the patterns.

In order to develop a theoretical basis for the above findings, we shall first investigate the properties of the diffusive reaction front in the presence of inhomogeneities in the initial distribution of the inner electrolyte. This is the simplest way to take into account the inhomogeneities and it allows us to obtain detailed understanding and analytical solutions. The ultimate goal, left for further studies, will be the use of the reaction zone results as an input to the description of the band formation in the spinodal decomposition scenario [21] which has been shown to correctly describe the pattern formation in the homogeneous case.

The paper in organized as follows. In section 2, we present a brief review of the main results known about the properties of diffusive reaction fronts in the case when the electrolytes are initially separated but otherwise are homogeneously distributed. Section 3 is devoted to the study of fronts when inhomogeneity is present in the initial state of the inner electrolyte. Both analytical results, at the mean-field level, as well as numerical results are given. Cellular automata simulations are presented in section 4 and the role of fluctuations is discussed.

2. Reaction front: homogeneous distribution of the inner electrolyte

We review here the properties of a reaction front emerging in an $A + B \to C$ process where the particles A and B diffuse and react with rate k upon contact. Initially, the reagents are separated, with the inner electrolyte B occupying the $x > 0$ half-space (homogeneously distributed with concentration b_0), while the outer electrolyte A is homogeneously distributed with concentration a_0 in the $x < 0$ half-space. Usually, the case $a_0 \gg b_0$ is considered and one finds that A and B react in a confined region (the reaction front) which moves in the positive x direction. The properties of this front can be addressed at different levels: a mean-field like one, neglecting fluctuations, or approaches that take the fluctuations into account.

[3] While the reagents in Liesegang phenomena are chemicals, examples where the reagents are of more exotic nature (such as topological defects [19]) are also known.

2.1. Mean-field analysis

The mean-field study of the front resulting from the reaction $A + B \to C$ has been made by Gálfi and Rácz [23]. The generalization to the reaction $nA + mB \to C$ has been given by Cornell *et al* [24]. We shall recall here the main results without going into the details of the calculations.

In the homogeneous initial condition case and with the fluctuations neglected, the concentration of the reagents $a(x, t)$ and $b(x, t)$ will depend only on the variable x at all times and the problem becomes one-dimensional. The reaction–diffusion equations for the concentrations $a(x, t)$ and $b(x, t)$ read

$$\partial_t a = D_a \partial_x^2 a - kab, \qquad \partial_t b = D_b \partial_x^2 b - kab, \tag{1}$$

where k is the reaction rate and D_a, D_b are, respectively, the diffusion coefficients of A and B.

The production rate of C, which is a quantity of interest since it is the source for the precipitation process in Liesegang phenomena [21], is obtained by computing $R(x, t) = ka(x, t)b(x, t)$. Actually, the region where $R(x, t)$ is significantly different from zero defines the reaction zone. The centre of the zone, $x_f(t)$, can be found from the condition $a(x_f, t) = b(x_f, t)$, and for the case of $D_a = D_b = D$ this leads to especially simple results. Indeed, one notices then that $u(x, t) = a(x, t) - b(x, t)$ obeys a simple diffusion equation. Introducing $q = b_0/a_0$, the solution is given in terms of the error function erf,

$$u(x, t) = a_0 \left[\frac{1 - q}{2} - \frac{1 + q}{2} \operatorname{erf}\left(\frac{x}{2\sqrt{Dt}} \right) \right] \tag{2}$$

and the condition $a(x_f, t) = b(x_f, t)$ yields

$$x_f(t) = \sqrt{2D_f t}. \tag{3}$$

This means that the front moves diffusively and its diffusion coefficient D_f is given by the equation $\operatorname{erf}(\sqrt{D_f/2D}) = (1 - q)/(1 + q)$.

In order to complete the description of the front one needs the solution of the nonlinear part of the reaction–diffusion equations,

$$\partial_t a = D\partial_x^2 a - k(a^2 + au). \tag{4}$$

It is not possible to obtain a general solution of this equation. However, assuming that the width $w(t)$ of the reaction front, defined as

$$w^2(t) = \frac{\int_{-\infty}^{\infty} (x - x_f)^2 R(x, t)\, \mathrm{d}x}{\int_{-\infty}^{\infty} R(x, t)\, \mathrm{d}x}, \tag{5}$$

is much smaller that the diffusion length $\ell_{\mathrm{diff}}(t) = \sqrt{2Dt}$ (an assumption that is justified *a posteriori*), one finds that, in the long-time limit, the quantities of interest take the following scaling forms in the reaction zone region:

$$\begin{aligned} &w(t) \sim t^{\alpha}, \qquad a(x, t) = t^{-\gamma} \hat{a}(xt^{-\alpha}), \\ &b(x, t) = t^{-\gamma} \hat{b}(xt^{-\alpha}), \qquad R(x, t) = t^{-\beta} \hat{R}(xt^{-\alpha}). \end{aligned} \tag{6}$$

Here the exponents are given as $\alpha = 1/6$, $\beta = 2/3$ and $\gamma = 1/3$. The exponents actually obey two general scaling relations following from the facts that $\ell_{\mathrm{diff}}(t) \gg w(t)$ and that the reaction zone is fed by the fluxes of diffusing particles [23, 24],

$$\alpha + \gamma = 1/2, \qquad 2\alpha + \gamma = \beta. \tag{7}$$

In the mean-field approximation, one has an extra scaling relation, namely $\beta = 2\gamma$, and this leads to the above values of the exponents. Note that the case $D_a \neq D_b$ is more complicated.

However, the exponents obey the same scaling relations, and only the scaling functions $\hat{a}$, $\hat{b}$, and $\hat{R}$ are affected.

A similar analysis can be carried out for the more general reaction $nA + mB \to C$ [24]. The main modification arises when expressing the production rate, and one has now the scaling relation $\beta = (n + m)\gamma$, leading to the mean-field exponents:

$$\alpha = \frac{n + m - 1}{2(n + m + 1)}, \qquad \beta = \frac{n + m}{n + m + 1}, \qquad \gamma = \frac{1}{n + m + 1}. \tag{8}$$

2.2. Beyond mean-field

Numerical simulations have been performed for the general reaction $nA + mB \to C$ [24], for several values of (n, m), including the case $n = m = 1$, and confirm the validity of the above scaling relations. Moreover, the mean-field exponents are recovered in dimensions larger than $d = 2$. In $d = 1$, the exponent values differ greatly from their mean-field values. This leads to the hypothesis that the upper critical dimension for diffusive reaction fronts is $d_u = 2$.

The validity of this hypothesis has been supported by theoretical arguments [25] based on the scaling behaviour of the steady-state front generated by imposing antiparallel fluxes of A and B particles. This situation is much easier to investigate, since the front is time independent, and depends only on three relevant parameters, the flux J, the diffusion coefficient D, and the reaction rate k. The results, however, can be directly applied to the time-dependent case too, since the front is formed quasistatically by diminishing fluxes $J(t) \sim t^{-1/2}$. Assuming that scaling applies even when fluctuations are present (as seen in numerical simulations), a dimensional analysis and scaling arguments lead to the following conclusions: first, there is an upper critical dimension $d_u = 2/(m + n - 1)$ above which mean-field predictions are correct; second, for $d < d_u$ (only realizable for $m = n = 1$), the width exponent is $\alpha = 1/2(d + 1)$, which for $d = 1$ gives $\alpha = 1/4$ instead of $\alpha = 1/6$ for the mean-field case.

In summary, one finds that, in the physically relevant dimensions, the reaction zone moves diffusively and its width is negligible with respect to the diffusion length of the problem. There is a third result which has not been discussed here but will be important in a later application when the front will figure as a source of particles in the description of the formation of Liesegang bands. Namely, the front leaves behind a constant concentration of C particles [23, 20].

3. Reaction front: inhomogeneous distribution of the inner electrolyte

There are many ways to introduce inhomogeneities. We shall consider here a simple case which, on one hand, can be treated analytically and, on the other hand, mimics a system with a geometrical inhomogeneity quite similar to the experimental setup used in [22]. Namely, we shall assume that the inhomogeneity is in the initial concentration of the inner electrolyte. As described in figure 1, the reagents are separated in the plane (x, y) into three zones, Σ_0, Σ_1, and Σ_2. For $x < 0$ and $\forall y$, $a = a_0$; $b = 0$ (region Σ_0), while for $x > 0$ the half-plane is divided in two domains, separated by a line making an angle θ with the x axis. In the upper domain Σ_1, $a = 0$; $b = b_{01}$, while in the lower domain Σ_2, $a = 0$; $b = b_{02}$. This corresponds to an engineered initial inhomogeneity of the reagent B.

As before we restrict ourselves to the reaction $A + B \to C$, although the results could be extended to the more general case $mA + nB \to C$. We also assume that the diffusion coefficients are equal: $D_a = D_b = D$.

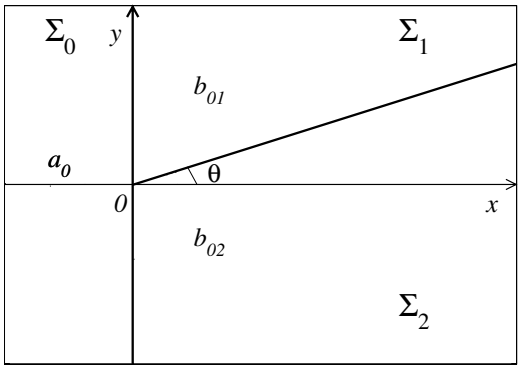

Figure 1. Geometry of the inhomogeneous media considered.

3.1. Mean-field description of the reaction front

The mean-field description is again in terms of the reaction–diffusion equations (1), the only difference being that the concentrations depend on two spatial variables (x, y) and the diffusion terms are now expressed through the two-dimensional Laplacian.

The position of the reaction front $(x_f(t), y_f(t))$ is again obtained by solving the diffusion equation for $u(x, y, t) = a(x, y, t) - b(x, y, t)$ and finding (x_f, y_f) satisfying the condition $u(x_f, y_f, t) = 0$. The diffusion equation being linear, the solution $u(x, t)$ for the initial condition in figure 1 can be constructed as a superposition of two particular solutions $u = u_1 + u_2$. Here $u_1(x, y, t)$ satisfies the initial condition $u_1(x < 0, y, t = 0) = a_0$ and $u_1(x > 0, y, t = 0) = -b_{01}$ and, according to equation (2), is given by

$$u_1(x, y, t) = a_0 \left[\frac{1 - q_1}{2} - \frac{1 + q_1}{2} \operatorname{erf}\left(\frac{x}{2\sqrt{Dt}} \right) \right] \tag{9}$$

where $q_1 = b_{01}/a_0$.

The second function $u_2(x, y, t)$ satisfies the initial condition $u_2 = 0$ in Σ_0 and Σ_1, and $u_2 = b_{01} - b_{02} = a_0(q_1 - q_2)$ in Σ_2 with $q_2 = b_{02}/a_0$. The solution is constructed in terms of the Green function for the diffusion operator

$$G(x, y, t) = \frac{1}{4\pi Dt} \exp\left(-\frac{x^2 + y^2}{4Dt} \right) \tag{10}$$

as an integral restricted to the region Σ_2:

$$u_2(x, y, t) = a_0(q_1 - q_2) \int_{\Sigma_2} \mathrm{d}x' \, \mathrm{d}y' \, G(x - x', y - y', t). \tag{11}$$

For simple cases, the integration can be performed analytically, leading to an explicit expression for u_2. For example, for the symmetric case when $\theta = 0$, one obtains

$$u(x, y, t) = a_0 \left\{ \frac{1 - q_1}{2} - \frac{1 + q_1}{2} \operatorname{erf}\left(\frac{x}{2\sqrt{Dt}} \right) + \frac{q_1 - q_2}{4} \left[1 + \operatorname{erf}\left(\frac{x}{2\sqrt{Dt}} \right) \right] \left[1 - \operatorname{erf}\left(\frac{y}{2\sqrt{Dt}} \right) \right] \right\}. \tag{12}$$

The position of the reaction front is thus given by the implicit equation:

$$\frac{1 - q_1}{2} - \frac{1 + q_1}{2} \operatorname{erf}(X_f) + \frac{q_1 - q_2}{4} \left[1 + \operatorname{erf}(X_f) \right] \left[1 - \operatorname{erf}(Y_f) \right] = 0, \tag{13}$$

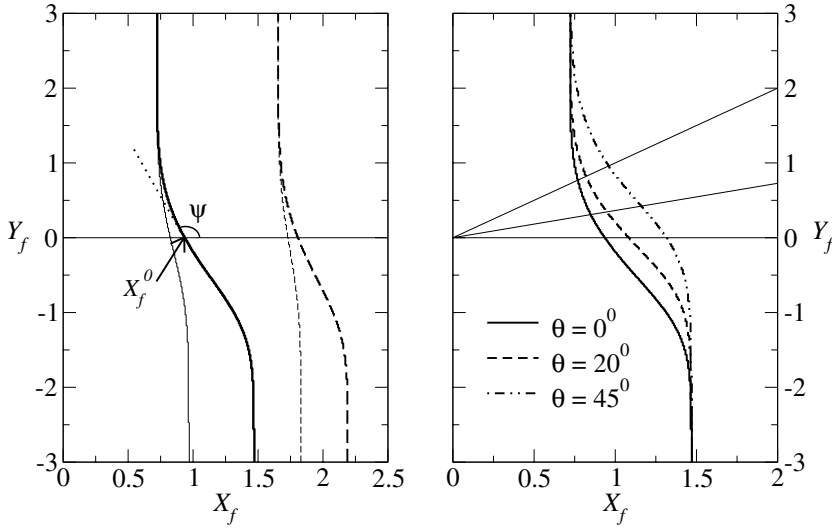

Figure 2. Shape of the reaction–diffusion front (in scaled time-independent variables) for different values of the parameters. Left panel: front shape for $\theta = 0$. The thick continuous line corresponds to $q_1 = 0.2$ and $q_2 = 0.02$; the thin continuous line to $q_1 = 0.2$ and $q_2 = 0.1$; thick dashed line: $q_1 = 0.01, q_2 = 0.001$; and thin dashed line: $q_1 = 0.01, q_2 = 0.005$. X_f^0 gives the intersection with the x axis, and ψ is the angle between the tangent at X_f^0 and the x axis. Right panel: front shape for different values of θ ($q_1 = 0.2$ and $q_2 = 0.02$). The thin straight lines indicate, respectively, the border between the regions Σ_1 and Σ_2 for the considered values of θ.

where

$$X_f = \frac{x_f(t)}{2\sqrt{Dt}}, \qquad Y_f = \frac{y_f(t)}{2\sqrt{Dt}} \tag{14}$$

are the scaled, *time-independent* coordinates of the front. The corresponding shape of the front is shown in the left panel of figure 2 for different values of the parameters q_1 and q_2.

Far from the x axis ($|y| \gg \sqrt{2Dt}$), the reaction front is not affected by the inhomogeneity; it is parallel to the y axis and moves diffusively, along the x direction. The diffusion coefficients are given, respectively, by $\mathrm{erf}(\sqrt{D_f^{1,2}/2D}) = (1 - q_{1,2})/(1 + q_{1,2})$.

Near the x axis, there is a crossover region between the two almost linear segments of the front. The crossover is smooth and can be characterized by the front position $x_f^0(t) = 2X_f^0\sqrt{Dt}$ on the x axis and by the angle ψ between the tangent to the front at X_f^0 and the x axis. The front position on the x axis is obtained from

$$\mathrm{erf}(X_f^0) = \frac{1 - (q_1 + q_2)/2}{1 + (q_1 + q_2)/2}, \tag{15}$$

and, of course, it also moves diffusively. The angle ψ on the other hand is a constant:

$$\tan\psi = -\frac{[1 + (q_1 + q_2)/2]^2}{q_1 - q_2}\exp[-(X_f^0)^2]. \tag{16}$$

A similar calculation can be performed for an arbitrary angle θ; however, the results can no longer be expressed in terms of explicit functions. Namely, the position of the front (in terms

of scaled variables) is given implicitly by the following equation:

$$\frac{2-q_1-q_2}{4}-\frac{2+q_1+q_2}{4}\,\mathrm{erf}(X_f) - \frac{q_1-q_2}{2\sqrt{\pi}}\int_{-\infty}^{X_f} \mathrm{d}z\ \exp(-z^2)\,\mathrm{erf}(Y_f - X_f\ \tan\theta - z\ \tan\theta) = 0. \tag{17}$$

The profile of the front is given in the right panel of figure 2 for different values of the angle θ. The analytical results have been checked by numerical integration of the reaction–diffusion equations for the reagents A and B. Note that the infinite reaction rate k limit is especially convenient for carrying out the numerical work since the position of the front does not depend on k for the $D_a = D_b$ case. However, it does not allow the investigation of the width of the front. For finite k, the width of the front in the asymptotic regions $Y_f \to \pm\infty$ follows from the case of homogeneous initial distribution of inner electrolyte, i.e. $w(t) \sim t^{\alpha}$ with $\alpha = 1/6$. Investigations of the crossover region in the case when fluctuations are also included (see next section) indicate that no anomalous behaviour occurs. Thus we expect that the width remains much smaller than the diffusion length and the scaling $w(t) \sim t^{\alpha}$ with $\alpha = 1/6$ remains valid everywhere along the front.

The conclusions one can draw from the analytic results and from figure 2 are as follows. First, the front motion remains diffusive but the shape deviates from straight line. Second, the distortion is smooth and can be parameterized by the two asymptotic limits at $Y_f \to \pm\infty$, and by a linear parameterization of the crossover region.

3.2. Beyond mean-field

To test whether the mean-field predictions are robust against including fluctuations, we will compare the above results to those given by a mesoscopic approach, namely by the simulation of the reaction–diffusion front by a cellular automaton. This approach also provides informations about how the width of the front scales with time, since a finite reaction rate is considered.

The model (described in more detail in [26] and [27]) is defined on a two-dimensional square lattice of 250 × 250 sites with synchronous dynamics at discrete time steps. One iteration of the automaton is defined as the combination of one diffusion and one reaction step. The diffusion coefficients for A and B particles are chosen to be equal, and the reaction $A + B \to C$ takes place only for particles entering a site from opposite directions. We use thus a finite reaction rate, since the probability for a reaction of two particles is equal to $1/4$. The front position is defined as the region where the difference of the two concentrations, computed in a Moore neighbourhood for the A and B particles, vanishes. To allow for better statistics the results are averaged over 750 runs.

The initial state is prepared as illustrated in figure 1. In the region Σ_0 (with a length of 100 sites), all the sites are fully occupied, i.e. the concentration of A particles is $a_0 = 1$. The regions Σ_1 and Σ_2 (of length of 150 sites) are randomly occupied by B particles with concentration $b_{01} = 0.2$ and $b_{02} = 0.02$, respectively.

The results of the cellular automata simulations for the case of $\theta = 0$ are shown in figure 3. We find good agreement between the analytical results and the averaged position of the front obtained from the cellular automata approach. The fluctuations in the system therefore appear to play no role for the position of the front. Equally good agreement was found for the case with a nonzero angle $\theta = 20°$.

Preliminary investigations of the time dependence of the width of the front at the separation line between Σ_1 and Σ_2 seems to indicate the same time scaling $w(t) \sim t^{1/6}$ as in the

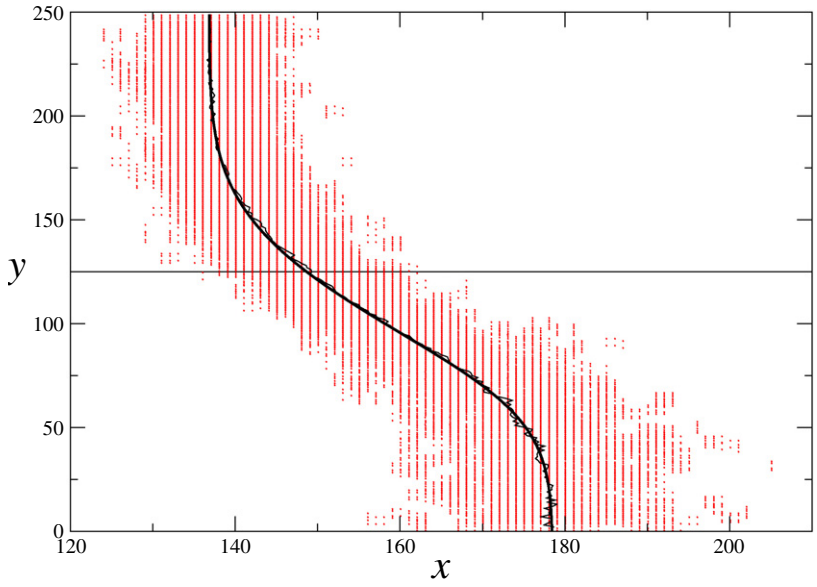

Figure 3. Results of the cellular automata simulations of the reaction–diffusion front for $\theta = 0$. The values of the initial concentrations are $a_0 = 1$, $b_{01} = 0.2$ and $b_{02} = 0.02$, and the diffusion coefficients for the A and B particles are equal $D_a = D_b$. The straight horizontal line separates the high- and the low-concentration regions of B particles. The points in the dotted region represent the instantaneous position of the front, calculated from condition $u = a - b = 0$ after 3000 timesteps. The thin noisy line gives the position of the front averaged over 750 realizations of the process. The analytic result is shown by the thick line.

(This figure is in colour only in the electronic version)

homogeneous case (as mentioned before, far from the inhomogeneity area the behaviour is obviously the one following from homogeneous initial distribution of the inner electrolyte).

4. Discussion

We have considered the motion of the reaction zone for a case of simple initial-state inhomogeneity which mimics the experimental setup where the Snell law had been discussed for Liesegang bands [22]. Our main finding is that although the straight-line shape of the front becomes distorted due to the inhomogeneity, the basic properties such as (1) the diffusive overall motion, (2) the negligible width, and (3) the irrelevance of fluctuations in the physical dimensions remain unchanged.

The next step towards understanding whether a version of the Snell law is valid for Liesegang bands meeting at a line of inhomogeneity should be the use of our present results as an input for a theory of Liesegang band formation. The best candidate should be the spinodal decomposition description which has been shown [21] to reproduce all the known generic properties of the Liesegang patterns.

Acknowledgments

This research has been partly supported by the Swiss National Science Foundation and by the Hungarian Academy of Sciences (Grants No. OTKA T043734 and TS 044839).

References

[1] van Saarloos W 2003 *Phys. Rep.* **386** 29
[2] Fisher R A 1937 *Ann. Eugenics* **7** 355
[3] Limat L *et al* 1992 *Physica* D **61** 166
[4] Swift J B and Hohenberg P C 1977 *Phys. Rev.* A **15** 319
[5] Kuramoto Y 1978 *Prog. Theor. Phys. Suppl.* **64** 346
[6] Cross M C and Hohenberg P C 1994 *Rev. Mod. Phys.* **65** 851
[7] Xin J 2000 *SIAM Rev.* **42** 161
[8] Mendez V *et al* 2003 *Phys. Rev.* E **68** 041105
[9] Zhabotinsky A M, Eager M D and Epstein I R 1993 *Phys. Rev. Lett.* **71** 1526
[10] Markus M and Stavridis K 1994 *Phil. Trans. R. Soc.* A **347** 601
[11] Sainhas J and Dilao R 1998 *Phys. Rev. Lett.* **80** 5216
[12] Muratov C B and Shvartsman S Y 2003 *Physica* D **186** 93
[13] Petrovskii S, Li B L and Malchow H 2003 *Bull. Math. Biol.* **65** 425
[14] Lane S L and Luss D 1993 *Phys. Rev. Lett.* **70** 830
[15] Sendina-Nadal I *et al* 1997 *Phys. Rev.* E **56** 6298
[16] Oosawa C and Kometani K 1996 *J. Phys. Chem.* **100** 11643
[17] Petrov V *et al* 1996 *J. Phys. Chem.* **100** 18992
[18] Henisch H K 1991 *Periodic Precipitation* (New York: Pergamon)
[19] Kuzoukov V and Kotomin E 1988 *Rep. Prog. Phys.* **51** 1479–1523
[20] Antal T, Droz M, Magnin J, Rácz Z and Zrinyi M 1998 *J. Chem. Phys.* **109** 9479
[21] Antal T, Droz M, Magnin J and Rácz Z 1999 *Phys. Rev. Lett.* **83** 2880
[22] Fialkowski M, Bitner A and Grzybowski A 2005 *Phys. Rev. Lett.* **94** 018303
[23] Gálfi L and Rácz Z 1988 *Phys. Rev.* A **38** 3151
[24] Cornell S, Droz M and Chopard B 1991 *Phys. Rev.* A **44** 4826
[25] Cornell S and Droz M 1993 *Phys. Rev. Lett.* **70** 3824
[26] Chopard B, Luthi P and Droz M 1994 *J. Stat. Phys.* **76** 661
[27] Chopard B and Droz M 1998 *Cellular Automata Modeling of Physical Systems* (Cambridge: Cambridge University Press)